Conformational Dynamics of the SH1-SH2 Helix in the Transition States of Myosin Subfragment-1

Lisa K. Nitao, Todd O. Yeates, and Emil Reisler
Department of Chemistry and Biochemistry and the Molecular Biology Institute, University of California, Los Angeles, California 90095 USA

ABSTRACT The α-helix containing the thiols, SH1 (Cys-707) and SH2 (Cys-697), has been proposed to be one of the structural elements responsible for the transduction of conformational changes in the myosin head (subfragment-1 (S1)). Previous studies, using a method that isolated and measured the rate of the SH1-SH2 cross-linking step, showed that this helix undergoes ligand-induced conformational changes. However, because of long incubation times required for the formation of the transition state complexes (S1.ADP.BeF_x, S1.ADP.AlF_4-, and S1.ADP.V_i), this method could not be used to determine the cross-linking rate constants for such states. In this study, kinetic data from the SH1-SH2 cross-linking reaction were analyzed by computational methods to extract rate constants for the two-step mechanism. For S1.ADP.BeF_x, the results obtained were similar to those for S1.ATPγS. For reactions involving S1.ADP.AlF_4- and S1.ADP.V_i, the first step (SH1 modification) is rate limiting; consequently, only lower limits could be established for the rate constants of the cross-linking step. Nevertheless, these results show that the cross-linking rate constants in the transition state complexes are increased at least 20-fold for all the reagents, including the shortest one, compared with nucleotide-free S1. Thus, the SH1-SH2 helix appears to be destabilized in the post-hydrolysis state.

INTRODUCTION

Myosin is a molecular motor that undergoes conformational changes, which are coupled to ATP hydrolysis and force generation. In an attempt to visualize these conformational changes, the myosin head has been crystallized in several nucleotide-bound states, including those representing both the prehydrolysis (MgATPγS, MgAMP.PNP, MgADP.BeF_x) and posthydrolysis (MgADP.V_i, MgADP.AlF_4-) states (Fisher et al., 1995; Gulick et al., 1997; Smith and Rayment, 1996). These structures of myosin fell into two main classes depending on the substructure of the 50-kDa cleft of the motor domain, the converter region, and the position of the lever arm. More recently, another structure of the myosin head has been determined. This structure was obtained using scallop muscle myosin complexed with MgADP and seems to represent a novel, third state of the cross-bridge cycle (Houdusse et al., 1999). In a comparison of these different states, the myosin head is represented by four subdomains, which are connected together by three "joints" serving as key structural elements (Houdusse et al., 2000). According to this model, the three joints coordinate the conformational changes that occur in the myosin head as it hydrolyzes ATP. One of these elements, located near the converter region of myosin, is a bent α-helix, which contains the reactive sulfhydryl groups, SH1 (Cys-707) and SH2 (Cys-697).

The SH1-SH2 helix has long been a focus of many biochemical studies. Early cross-linking studies demonstrated that when nucleotides (MgADP or MgATPγS) are bound to subfragment-1 (S1), the rate of SH1-SH2 cross-linking is increased (Reisler et al., 1974; Wells et al., 1980). Crystallographic evidence for the nucleotide-induced destabilization of the SH1-SH2 helix has been obtained so far only from the scallop S1.ADP structure (Houdusse et al., 1999). In this structure, the electron density of the SH1-SH2 region could not be defined, suggesting that the helix is disordered and that its order-disorder transitions may be functionally important. In fact, the SH1-SH2 helix has been shown in several prior studies to impact the function of myosin. Myosins with glycine residues in the helix mutated to alanines have altered ATPase activities and show a complete loss of the motor function (Kinose et al., 1996; Patterson et al., 1997). Similarly, the modification of either SH1 or SH2 has resulted in the loss of myosin function (Root and Reisler, 1992; Marriott and Heidecker, 1996). These and similar results suggest that the SH1-SH2 helix undergoes conformational changes and that the flexibility of this helix may be important for the proper function of myosin.

In our previous studies, we probed the conformational changes occurring within the SH1-SH2 helix by monitoring the kinetic rates of its cross-linking. To do so, we developed a method that isolates the cross-linking reaction; therefore, enabling the direct measurement of its rate (Nitao and Reisler, 1998). In this way, we have shown that the SH1-SH2 cross-linking rate is affected by several factors, including the cross-linking span of the reagent, the presence of ligands (nucleotides and/or actin) and temperature (Nitao and Reisler, 2000). Our results suggested a flexible (or melted) conformation of the SH1-SH2 helix in the prehydrolysis state of S1 (represented by the S1.ATPγS state) and

Submitted April 5, 2002, and accepted for publication June 27, 2002.

Address reprint requests to Emil Reisler, Department of Chemistry and Biochemistry and the Molecular Biology Institute, University of California, Los Angeles, CA 90095. Tel.: 310-825-2668; Fax: 310-206-7296; E-mail: reisler@mbi.ucla.edu.

0006-3495/02/11/2733/09 $2.00

a highly stabilized helix in the acto-S1 and acto-S1.ADP complexes. However, due to experimental complications, we could not measure the cross-linking rates in the transition states of S1, specifically those represented by S1.ADP.BeF_x, S1.ADP.AlF_4-, and S1.ADP.V_i. There is some evidence for conformational differences of this helix in the transition states. From the comparison of the structures of different nucleotide-bound states of scallop S1, it appears that the SH1-SH2 helix is transformed from a highly flexible structure in the "ATP state" (S1.ADP) into a rigid one in the prepower stroke state (S1.ADP.V_i) (Houdusse et al., 2000). In principle, cross-linking experiments should provide insight into the conformational dynamics of this helix in the transition states of S1 and ATP in solution.

In this work, a different approach for determining the cross-linking rates of SH1 and SH2 in the transition states of S1 was adopted. By measuring different components of the two-step modification reaction (via ATPase activity and acto-S1 binding assays) and analyzing the kinetic data by computer methods, we were able to obtain the rates of its individual steps (SH1 modification and SH2 cross-linking). The results from this analysis indicate that MgADP.BeF_x has a similar effect on the SH1-SH2 helix to that of MgATPγS. The rate of cross-linking increases only several-fold compared with that in apoS1 for the shortest reagent, whereas rate increases for the longer reagents are much greater. The results obtained for the S1.ADP.AlF_4- and S1.ADP.V_i states were more surprising. These states show elevated cross-linking rates for all of the reagents, including the shortest one. This suggests that the SH1-SH2 helix may be flexible also in the posthydrolysis state.

MATERIALS AND METHODS

Reagents

N-Ethylmaleimide (NEM), ADP, and Sephadex G-50 were purchased from Sigma (St. Louis, MO). *N*,*N*′-1,2-phenylene dimaleimide (oPDM) and *N*,*N*′-1,4-phenylene dimaleimide (pPDM) were purchased from Research Organics (Cleveland, OH). *N*,*N*′-1,3-phenylene dimaleimide and 1,1′-(methylenedi-4, 1-phenylene) bismaleimide (BM) were purchased from Aldrich (Milwaukee, WI). Adenosine-5′-(3-thiotriphosphate) (ATPγS) was obtained from Boehringer Mannheim (Germany).

Proteins

Actin and myosin were obtained from rabbit psaos muscle as described previously (Godfrey and Harrington, 1970; Spudich and Watt, 1971). S1 was prepared by the chymotryptic digestion of myosin filaments as described before (Weeds and Pope, 1977). The concentration of S1 and actin were determined spectrophotometrically by using the extinction coefficients of $E^{1\%}_{280} = 7.5\ cm^{-1}$ and $E^{1\%}_{292} = 11.5\ cm^{-1}$, respectively.

Formation of the phosphate analog complexes in S1

The complexes of S1 with phosphate analogs were formed by incubation of S1 with 1.0 mM MgADP and either 5.0 mM NaF + 0.5 mM $BeCl_2$, or 10 mM NaF + 0.5 mM $AlCl_3$, or 1.0 mM NaV_i (Phan et al., 1996; Goodno, 1982). In the SH2 modification experiments, these complexes were formed after SH1 on S1 was modified with NEM. In other cases, the complexes were formed with unmodified S1, after which the modification experiments were carried out on the S1 complexed with either ADP + BeF_x, ADP + AlF_4-, or ADP.V_i. ATPase activities of the S1 complexes were measured to determine the extent of complex formation. In each case, the extent of complex formation was at least 90%.

ATPase activities

As described previously, Ca^{2+}- and EDTA- (K^+-) ATPase activities of S1 were determined at 37°C (Nitao and Reisler, 1998). The Ca^{2+}-ATPase assay solution contained 600 mM KCl, 50 mM Tris-HCl (pH 7.6), 5.0 mM $CaCl_2$, and 2.0 mM ATP. The EDTA-ATPase assay solution contained 444 mM KCl, 50 mM histidine, 50 mM Tris-HCl (pH 7.6), 5.0 mM EDTA, and 2.0 mM ATP.

Cross-linking experiments for computational analysis

Because of the difficulty in determining the cross-linking rates using our previous spin column method, the cross-linking rates for the transition states of ATP were determined by using numerical computer methods to fit the model kinetic data to the observed kinetic data. To test the validity of these calculations, we applied them first to the SH1-SH2 cross-linking reactions in the S1.ADP and S1.ATPγS states, which were investigated before. The cross-linking experiments were designed to provide two sets of data that are needed for the kinetic analysis: the extent of SH1 modification and SH1-SH2 cross-linking. As in many previous studies, the extent of SH1 modification was obtained from EDTA ATPase activity assays (Sekine and Kielley, 1964) and the cross-linking extent was determined from acto-S1 binding measurements (Polosukhina and Highsmith, 1997). The first step in these reactions involved the modification of S1 by the cross-linking reagent (oPDM, pPDM, BM in dimethylformamide). The reagent (150 μM) was added to S1 (30 μM) in a buffer containing 10 mM NaCl, 10 mM PIPES, pH 7.0, and 1.0 mM nucleotide (MgADP or MgATPγS), if present. At various time points, aliquots of the reaction were quenched with 1.0 mM dithiothreitol (DTT). The EDTA ATPase activity of each time point was measured to determine the amount of S1 that was modified at SH1. As in previous studies (Nitao and Reisler, 1998), the decreases in EDTA ATPase activity over the time course of all modification reactions were attributed to the modification of SH1 on S1.

In the next step, the amount of cross-linked S1 was measured. To do so, each aliquot was split into two equal portions. A threefold excess of actin was added to one set of samples, while an equal volume of buffer was added to the other set of samples. Then, the concentration of NaCl was raised to 100 mM in all of the samples. This was done to ensure that only the strongly binding S1 (unreacted and SH1-modified S1) and not the weakly binding S1 (cross-linked S1) will be bound to the actin. At this point, the final concentration of S1 and actin are 10 and 30 μM, respectively. After the samples were allowed to incubate overnight (at 4°C), each sample was spun for 15 min in a Beckman airfuge (140,000 $\times$ *g*). The supernatant was then removed to determine the amount of S1 in solution. The amount of S1 in each sample was measured via the tryptophan fluorescence, using excitation and emission wavelengths of 295 and 340 nm, respectively. Such measurements on the supernatants of samples containing actin yielded the amount of cross-linked S1 formed during the reaction, whereas the samples without actin provided a normalization factor (i.e., total amount of S1 in each sample).

For the reactions in the presence of the phosphate analogs, there were minor adjustments to the above protocol. After the formation of the phosphate analog complexes with S1, the cross-linking reagent (150 μM) was added to the complexed S1 (30 μM). Reaction aliquots were quenched

with DTT at various time points. Each sample was spun through a Sephadex G-50 column, equilibrated with 10 mM NaCl, 10 mM PIPES, pH 7.0 to remove the excess NaV_i or NaF and $BeCl_2$ or $AlCl_3$. The concentration of S1 in each time point was determined by using Bradford assay (Bradford, 1976). At this point, the samples were split into two parts. A threefold molar excess of actin (30 μM) was added to one set of samples (10 μM S1), while an equal volume of buffer was added to the other set. Because the formation of the complexes inhibits ATPase activity, this measurement could only take place after actin was added to the samples to release the bound nucleotide and phosphate analogs. The EDTA ATPase activity of each reaction time point was measured using the samples that contained actin. Comparison of the ATPase activity of the initial time point with that of uncomplexed S1 (that had undergone the same treatment) revealed the complete removal of the phosphate analog complexes from S1. The amount of cross-linked S1 was then determined via tryptophan fluorescence as described in the previous section.

Reaction rate determination by numerical computer methods

The modification of S1 with a bifunctional cross-linking reagent can be described by Scheme 1:

$$A + B \underset{k_1}{\rightarrow} C \underset{k_2}{\rightarrow} D$$

in which *A, B, C,* and *D* represent the concentrations of S1, cross-linking reagent, SH1-modified S1, and SH1-SH2 cross-linked S1, respectively. The rate constants are represented by k_1 for the rate of SH1 modification and k_2 for the rate of cross-linking. The first step (SH1 modification) is a second order reaction, which is followed by the cross-linking to SH2, a pseudo-first order reaction. Because an analytical solution for this reaction scheme cannot be easily applied to rate determinations, numerical methods were used to establish values for the rate constants that gave optimal agreement with the experimental data on the concentrations of S1 and cross-linked S1 versus reaction time.

For each experiment, the values of k_1 and k_2 were determined according to least-squares criteria. Initial estimates of k_1 and k_2 were obtained by linear least-squares from sets of equations of the following form:

$$\frac{d[C]_i}{dt} = [A]_i[B]_i k_i - [C]_i k_2 \quad (1)$$

$$\frac{d[A]_i}{dt} = -[A]_i[B]_i k_1 \quad (2)$$

The subscript *i* denotes the time point. The derivatives were estimated numerically from concentrations at sequential time points.

The final values of k_1 and k_2 were obtained by iterative nonlinear least squares, minimizing the discrepancy between measured and calculated (simulated numerically) values of [*A*] and [*D*]. For most experiments, the estimated uncertainties in k_1 and k_2 were approximately 10%.

For certain conditions, the relative rates of the two steps were such that the intermediate [*C*] did not accumulate to a measurable extent. As a result, k_2 could not be determined with precision. However, even in these cases, it was possible to establish a lower limit on the value of k_2 with further numerical simulations.

5,5′-Dithio-bis-(2-nitrobenzoic acid) (DTNB) titration experiments

The modification of S1.ADP.V_i with pPDM was performed as described in the previous section. After terminating the cross-linking in reaction aliquots with DTT, the excess reagent and DTT were removed on Sephadex G-50 spin columns, which were equilibrated with the reaction buffer. The concentration of S1 in each sample was determined using the Bradford assay. Unmodified and modified S1 (3.0 μM) were denatured in 6 M urea, 50 mM Tris, pH 8.0 for 15 min at 60°C. After the samples were cooled to room temperature, DTNB (300 μM) was added. After 15 min, the optical density of the samples were measured at 412 nm, and the unmodified cysteines were determined by using a molar extinction coefficient of 14,290 M^{-1} cm^{-1} (Ellman, 1959; Riddles et al., 1983).

SH2 modification rates

SH2 modification rates were determined as described previously with some modification due to the use of the phosphate analog complexes (Nitao and Reisler, 1998). SH1 was modified by adding a fivefold excess of NEM over S1 (20–25 μM). After 90 min, the reaction was stopped with the addition of 1.0 mM DTT. All SH1 modification reactions were carried out in 10 mM KCl, 10 mM PIPES, pH 7.0. SH1-NEM S1 was then dialyzed overnight in 10 mM KCl, 10 mM PIPES, pH 7.0 to remove any excess reagent and DTT. For reactions not containing the phosphate analogs, SH1-NEM S1 (10 μM) was modified by adding a fourfold excess of cross-linking reagent (oPDM, pPDM, BM). At selected time intervals, the modification reactions were quenched in aliquots containing 1.0 mM DTT. For reactions containing the phosphate analog complexes, the complexes were formed with SH1-NEM S1 (10 μM) as described in a previous section. The extent of complex formation was determined by the loss of Ca^{2+}-ATPase activity. Under these conditions, 95% to 100% of the Ca^{2+}-ATPase activity was lost, indicating a nearly complete formation of the phosphate analog complexes. After the formation of the complexes, a fourfold excess of cross-linking reagent was added. At different time points, the modification reactions were quenched in aliquots containing 1.0 mM DTT. Because phosphate analogs inhibit the Ca^{2+}-ATPase activity of S1, they had to be removed to determine the rate of SH2 modification by the Ca^{2+}-ATPase activity assay. To do so, each time point aliquot was applied to a spin column equilibrated with 10 mM KCl, 10 mM PIPES, pH 7.0. This removed all of the NaF and $BeCl_2$ or $AlCl_3$ not bound to S1. Once the S1 concentration in each aliquot was determined (Bradford assay), a threefold excess of actin was incubated with S1 overnight to release the bound phosphate analog complexes from S1 (the complete removal of the phosphate analog complexes from S1 was verified in control experiments). Then, the Ca^{2+}-ATPase activity of each reaction time point was measured. The Ca^{2+}-ATPase activities of the modified samples were plotted versus reaction time to determine the first-order rate constants of SH2 modification.

RESULTS

Experimental approach

In both structural and solutions studies, the transition states of S1 and ATP are represented by the nucleotide and phosphate analog complexes ADP.BeF_x, ADP.AlF_4-, and ADP.V_i. The first step in the formation of these complexes involves the binding of ADP to S1, which accelerates the cross-linking to SH2 when bifunctional reagents are attached to SH1. Consequently, by the time the slow formation of phosphate analog complex is completed, all of the SH1-modified S1 would be cross-linked, precluding any measurements of SH1-SH2 cross-linking in the transition state analog state. Due to this experimental difficulty, the cross-linking rates could not be measured for the transition state complexes of S1 using the spin column isolation of the cross-linking reaction (Nitao and Reisler, 1998).

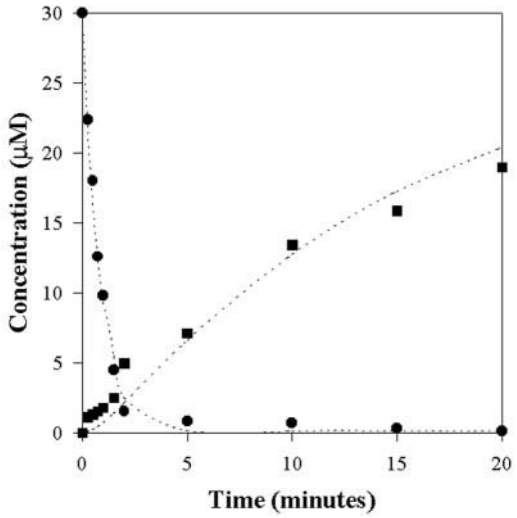

FIGURE 1 Progress of pPDM modification of S1. For these experiments, S1 (30 μM) was reacted with pPDM (150 μM) in a buffer containing 10 mM NaCl, 10 mM PIPES, pH 7.0 at 25°C. For each time point, the concentrations of S1 (●) and SH1-SH2 cross-linked S1 (■) were measured as described in the Material and Methods. The dotted line represents the curve drawn through the values of S1 and cross-linked S1 that were determined from the numerical computer simulation, using k_1 and k_2 values of 141 M^{-1} s^{-1} and 7.95 ($\times 10^{-4}$) s^{-1}, respectively.

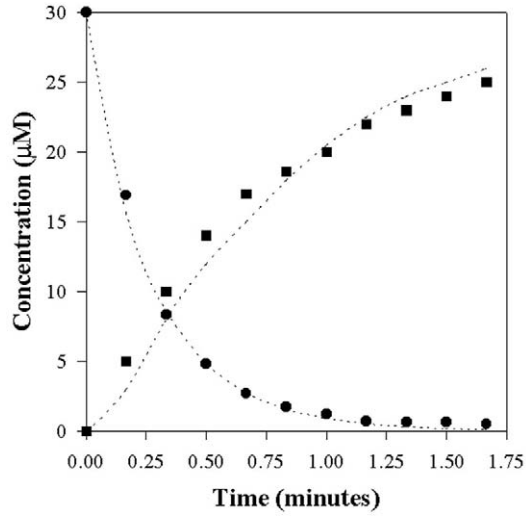

FIGURE 2 Progress of pPDM modification of S1.ADP. For each time point, the concentrations of S1 (●) and cross-linked S1 (■) were measured. The dotted line represents the curve drawn through the values of S1 and cross-linked S1 that were determined from the numerical computer simulation, using k_1 and k_2 values of 337 M^{-1} s^{-1} and 340 ($\times 10^{-4}$) s^{-1}, respectively.

In this study, an alternative approach has been taken to determine the cross-linking rates. The two steps of the reaction (SH1 modification and SH2 cross-linking) were analyzed using numerical computer methods. For this computer modeling approach, the concentrations of unmodified S1 (A, reactant) and SH1-SH2 cross-linked S1 (D, SH1-X-SH2) had to be measured at different time points of the reaction. These concentrations were determined throughout the reaction for each reagent and nucleotide state tested. These data points were then used to extract the rate constants for SH1 modification (k_{1X}) and SH2 cross-linking (k_{2X}) as described in Materials and Methods. Then, using these calculated rate constants, the corresponding concentrations of S1 and cross-linked S1 at the various time points were recalculated for comparison in a simulated reaction. The simulated curves describing the recalculated S1 and SH1-X-SH2 concentrations were then plotted along with the experimental data against the reaction time. Figs. 1 and 2 show reaction profiles generated for the pPDM modifications of S1 and S1.ADP, respectively. From these plots, it appears that the simulated curves provide adequate descriptions of the reaction in Scheme 1 and thus, the rate constants derived from these simulations report the rates of these reactions.

Rates of SH1 modification

The rate constants for SH1 modification (k_{1X}) in the presence (k_{1N}) and absence (k_1) of nucleotide, and the ratios of these constants (k_{1N}/k_1) are given in Table 1. These ratios give a better insight into the effect that a particular nucleotide state analog has on the rate of SH1 modification. Three reagents and five nucleotide states were tested. Any particular nucleotide or nucleotide-state analog had similar effects on the rate constants for the SH1 reaction with the three reagents. In the ADP and ATPγS states of S1, the rate for SH1 modification increased severalfold. In the ADP-.BeF_x state, there was either no effect (pPDM, BM) or an increase (oPDM) in the rate of SH1 modification. For the nucleotide analogs representing the posthydrolysis state of S1 (ADP.AlF_4- and ADP.V_i), the rates of SH1 modification were greatly inhibited. These results agree well with those published previously, in which the effect of different nucleotide states on SH1 modification were determined for different reagents (Phan et al., 1997; Hiratsuka et al., 1998).

Rates of SH2 modification

To ensure that the effects observed in cross-linking are not due to differences in the ability to modify SH2, the rates of SH2 modification were determined for each cross-linking reagent on SH1-modified S1. These rates, shown in Table 2, were determined for the states represented by the analogs, ADP.BeF_x and ADP.AlF_4-. By comparing the ratios of the rates in the presence over absence of nucleotide, it appears that modification of SH2 by each reagent is similarly increased, fourfold to sixfold for the ADP.BeF_x state. For the ADP.AlF_4- state, the rates of SH2 modification were all inhibited, approximately 60% of the nucleotide-free state. Although SH2 modification is inhibited in the posthydroly-

TABLE 1 SH1 modification rates in the presence (k_{1N}) and absence (k_1) of nucleotides at 25°C

Reagent (cross-linking span)	Nucleotide added	k_{1X} (M^{-1} s^{-1})	k_{1N}/k_1
oPDM (9.39 ± 0.47 Å)	-	34.0 ± 4.3	-
	MgADP	115.3 ± 18.2	3.4 ± 0.9
	MgATPγS	204.0 ± 40.6	6.0 ± 1.9
	MgADP.BeF_x	102.5 ± 12.7	3.0 ± 0.7
	MgADP.AlF_4−	1.70 ± 0.05	0.05 ± 0.01
	MgADP.V_i	1.74 ± 0.05	0.05 ± 0.01
pPDM (11.13 ± 0.52 Å)	-	133.1 ± 11.0	-
	MgADP	353.8 ± 38.0	2.7 ± 0.5
	MgATPγS	456.1 ± 42.2	3.4 ± 0.6
	MgADP.BeF_x	104.4 ± 9.3	0.8 ± 0.1
	MgADP.AlF_4−	4.28 ± 0.16	0.03 ± 0.004
	MgADP.V_i	3.80 ± 0.17	0.03 ± 0.004
BM (14.53 ± 1.51 Å)	-	126.0 ± 10.9	-
	MgADP	535.6 ± 61.6	4.2 ± 0.8
	MgATPγS	608.4 ± 45.0	4.8 ± 0.8
	MgADP.BeF_x	133.5 ± 10.5	1.1 ± 0.2
	MgADP.AlF_4−	6.92 ± 0.32	0.05 ± 0.01
	MgADP.V_i	8.75 ± 0.53	0.07 ± 0.01

All rate constants were determined by numerical computer simulations of reactions in which S1 was modified by the cross-linking reagent. The cross-linking spans of each reagent, determined using a stochastic molecular dynamics method, are from a recent study by Green et al., 2000. Each rate constant (k_{1X}) is the mean value of at least three independent experiments. k_{1N}/k_1 represents the ratio of cross-linking rate constants of S1 in the presence of nucleotide (k_{1N}) versus S1 alone (k_1).

sis states, the cross-linking does not appear to be similarly affected, as discussed in the following section.

Estimated rate constants of SH1-SH2 cross-linking

The rate constants for SH1-SH2 cross-linking (k_{2X}) and the ratios of cross-linking in the presence (k_{2N}) over the absence (k_2) of nucleotide are shown in Table 3 for each reagent and nucleotide-bound state. These data were obtained from reaction simulations similar to those shown in Figs. 1 and 2. The results obtained for SH2 cross-linking appear to fall into two classes: the states representing the posthydrolysis state (ADP.AlF_4− and ADP.V_i) and the remaining states (ADP, ATPγS, ADP.BeF_x). For all nucleotide-bound states other than ADP.AlF_4− and ADP.V_i, the results followed the patterns that were described in our previous study (Nitao and Reisler, 1998). The cross-linking rates increased severalfold for the shortest reagent (oPDM) and much more for the longer reagents (pPDM, BM), between 35- and 65-fold.

TABLE 2 SH2 modification rates in the presence and absence of nucleotides at 25°C

Reagent	k_{SH2} (min^{-1})	k_{SH2N} (min^{-1})	k_{SH2N}/k_{SH2}
		MgADP.BeF_x	
oPDM	0.005 ± 0.001	0.019 ± 0.002	4.0 ± 1.2
pPDM, BM	0.019 ± 0.005	0.115 ± 0.025	6.0 ± 2.9
		MgADP.AlF_4−	
oPDM	0.005 ± 0.001	0.0033 ± 0.0005	0.66 ± 0.23
pPDM, BM	0.019 ± 0.010	0.012 ± 0.002	0.63 ± 0.30

All rate constants were obtained from semilogarithmic plots of the Ca^{2+}-ATPase activity of modified S1 versus time of reaction. The rates are the mean values of at least two independent experiments. k_{SH2} represents the rate constant of SH2 modification in the absence of nucleotide. k_{SH2N} represents the rate constant of SH2 modification in the presence of the transition state analog complexes. The errors are the mean deviations of several rate determinations from the mean value of rate constants.

TABLE 3 Cross-linking rates in the presence (k_{2N}) and absence (k_2) of nucleotide at 25°C

Reagent	Nucleotide added	k_{2X} ($\times 10^{-4}$ s^{-1})	k_{2N}/k_2
oPDM	-	4.8 ± 0.5	-
	MgADP	19.9 ± 3.8	4.1 ± 1.4
	MgATPγS	27.3 ± 4.7	5.6 ± 1.8
	MgADP.BeF_x	16.6 ± 2.0	3.4 ± 1.0
	MgADP.AlF_4−	≥100	≥21
	MgADP.V_i	≥100	≥21
pPDM	-	7.6 ± 0.8	-
	MgADP	323 ± 31	43 ± 10
	MgATPγS	460 ± 43	61 ± 13
	MgADP.BeF_x	356 ± 34	47 ± 11
	MgADP.AlF_4−	≥200	≥26
	MgADP.V_i	≥200	≥26
BM	-	9.5 ± 0.8	-
	MgADP	397 ± 35	42 ± 7
	MgATPγS	559 ± 52	59 ± 10
	MgADP.BeF_x	613 ± 81	65 ± 14
	MgADP.AlF_4−	≥300	≥32
	MgADP.V_i	≥300	≥32

All rate constants were determined from numerical computer simulations of reactions in which S1 was modified by cross-linking reagent. Each rate constant is the mean value of at least three independent experiments. k_{2X} represents the rate constant of cross-linking in the absence (k_2) or presence (k_{2N}) of nucleotide. For the ADP.AlF_4− and ADP.V_i states of S1, only lower limits of these rate constants were established.

For the posthydrolysis states, the results obtained for the cross-linking rates were more complex. Due to the strong inhibition of SH1 modification in these states, this first reaction in Scheme 1 became the rate-limiting step of the overall reaction (in the other states, the SH1 modification occurred sufficiently fast such that the cross-linking reaction was the rate-limiting step). Furthermore, the slower reaction kinetics of SH1 modification could allow for other thiols on S1 to be modified by the cross-linking reagent. To address this issue, DTNB titration experiments were performed using reaction aliquots from the pPDM modification of S1.ADP.V_i. By comparing the changes in EDTA ATPase activity (indicating the amount of S1 modified) with the amount of thionitrobenzoic acid released (indicating the amount of free cysteine groups), the number of cysteines lost at different time points of the reaction can be determined. The results showed that approximately one cysteine was lost for a sample that had a 50% decreased EDTA ATPase activity, and two cysteines were modified upon a ~90% loss of activity. This loss of cysteines is consistent with SH1-SH2 cross-linking.

Because of the difficulty presented by the slow modification of SH1, the analysis could not provide the actual rate constant for cross-linking in the ADP.AlF_4− and ADP.V_i states. However, reaction simulations could establish the lower limits for k_2 values by comparing the simulated curves with the experimental results. Examples of this analysis are shown in Figs. 3 and 4. Fig. 3 shows the oPDM modification reaction for the S1.ADP.AlF_4− state. The solid circles corresponds to the experimental concentrations of SH1-X-SH2, whereas the dotted lines represent the simulated curves in which the k_2 values were set at 0.04, 0.02, 0.01, 0.005, 0.0025, and 0.0012 s^{-1} and k_1 was kept constant at its estimated value of 1.46 ± 0.03 M^{-1} s^{-1}. At k_2 = 0.04 s^{-1} (open squares) or for other values of k_2 above ~0.01 s^{-1}, the simulated curve agrees rather well with the experimental values. As k_2 is decreased to 0.005 s^{-1} (open diamonds) and beyond, the simulated curves shift away from the experimental values, indicating that the lower limit for k_2 is approximately 0.01 s^{-1} for this experimental data set (open triangles pointed down). As evident from the inset to Fig. 3, the time-dependent changes in the measured concentrations of unlabeled S1 are simulated well by the selected rate constants (Fig. 3). Fig. 4 shows the data for pPDM cross-linking in the ADP.AlF_4− state. Again, when the k_2 value is 0.04 s^{-1} (open squares) and k_1 is 3.09 ± 0.07 M^{-1} s^{-1}, the simulated curves provide the best descriptions of the experimental data for the concentrations of unlabeled and cross-linked S1. In this case, the simulated curve begins to deviate from the experimental values when the k_2 value drops to and below 0.01 s^{-1} (open triangles pointed down). This suggests that the lower k_2 limit for this pPDM experiment is approximately 0.02 s^{-1} (open triangles pointed up). This analysis was repeated for all of the experiments that involved the nucleotide states, ADP.AlF_4− and ADP.V_i.

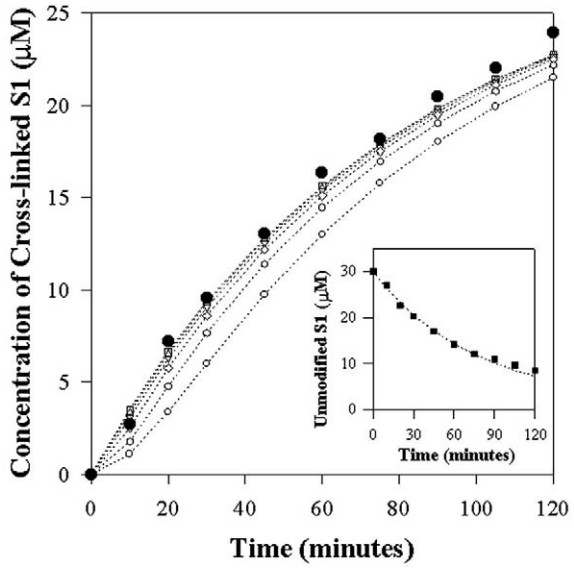

FIGURE 3 Progress of oPDM modification of S1.ADP.AlF_4−. The concentrations of cross-linked S1 are shown (●) in the main plot with the unmodified S1 values in the inset (■). For this data set, the k_1 value was determined to be 1.46 ± 0.03 M^{-1} s^{-1}. The dotted line (*inset*) represents the curve drawn through the values of S1 that were determined from the numerical computer simulation. To determine the lower limit of k_2 values for this reaction, the kinetic simulations were performed by keeping the k_1 value constant at 1.46 ± 0.03 M^{-1} s^{-1} and setting the k_2 value at 0.04 (□), 0.02 (△), 0.01 (▽), 0.005 (◇), 0.0025 (○), or 0.00125 (○) s^{-1}. Dotted lines in the main plot represent the curves drawn through the values of cross-linked S1 that were determined from the numerical computer simulation.

The ratios of cross-linking rates were calculated using the lower limit k_2 values obtained from such analysis of reactions in the posthydrolysis states. These ratios (Table 3) reveal that although the SH1 and SH2 modifications are inhibited to different degrees in the S1.ADP.AlF_4− and S1.ADP.V_i complexes, the cross-linking reaction is strongly accelerated relative to that in the apo S1. Also, in contrast to the other nucleotide states (ADP, ATPγS, ADP.BeF_x), there appears to be a significant increase in the rate of cross-linking with oPDM (~20-fold) for both the S1.ADP.AlF_4− and S1.ADP.V_i states. pPDM and BM also yield similar lower limits for the k_{2N}/k_2 ratios (between 20 and 30).

DISCUSSION

In our previous studies, we probed the conformational changes of the SH1-SH2 helix in different nucleotide-bound states. To do so, we used five different reagents as rulers of distances. Since then, stochastic molecular dynamics calculations were done to determine accurately the spans of various cross-linking reagents (Green et al., 2001). The new values for the spans of the three cross-linking reagents used in this study are listed in Table 1. These values represent the cross-linking distances that are most populated in an aqueous environment, but the range of distances that each re-

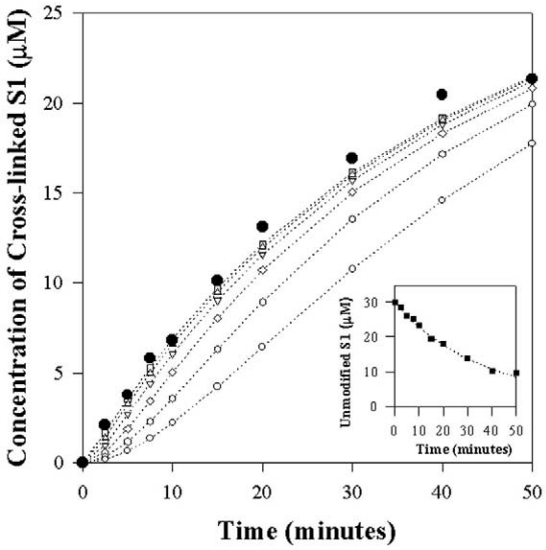

FIGURE 4 Progress of pPDM modification of S1.ADP.AlF_4^-. The experimental values obtained for the concentration of cross-linked S1 (●) are shown in the main plot with the unmodified S1 values (■) in the inset. The k_1 value in this experiment was determined to be 3.09 ± 0.07 M^{-1} s^{-1} (*inset*). The dotted line (*inset*) represents the curve drawn through the values of S1 that were determined from the numerical computer simulation. Again, kinetic simulations were performed in which k_1 was set at 3.09 ± 0.07 s^{-1} and k_2 varied from 0.04 (□), 0.02 (△), 0.01 (▽), 0.005 (◇), 0.0025 (○), and 0.00125 (○) s^{-1}. The dotted lines in the main plot represent the curves drawn through the values of cross-linked S1 that were determined from the numerical computer simulation.

agent occupies is much greater (7.67–10.46 Å, 9.20–12.29 Å, and 9.40–17.43 Å for oPDM, pPDM, and BM, respectively). The new values indicate that the conformations that the SH1-SH2 helix adopts are under stricter distance constraints than previously believed.

In the present study, kinetic experiments were analyzed by numerical methods to determine the cross-linking rates in the transition states of S1. To gain confidence in this method, experiments were also performed using nucleotide states for which the cross-linking rates were determined in a previous study after separating the two steps of the reaction (Nitao and Reisler, 1998). Although the numerical values of k_{2N}/k_2 are not the same in all cases, the trends observed in this work agree with those seen in the previous study. SH1-SH2 cross-linking with oPDM is only increased severalfold, whereas the increases in cross-linking rates were much greater for the longer reagents in the ADP and ATPγS states (Nitao and Reisler, 1998). Although ATPγS does induce a greater destabilization of the helix (as seen from the larger k_{2N}/k_2 ratio), the differences between these two states are smaller than in the previous study.

Clearly, the numerical analyses of the kinetic data do not yield as accurate rate constants as the direct determinations of k_2 for the isolated (by spin column) cross-linking reaction. This is apparent from the imperfect fit of the simulated curves of S1 and SH1-X-SH2 concentrations to the experimental data in Figs. 1 and 2. One contributing factor is that the measurement of SH1-X-SH2 via the actin-binding assay, which involves several steps of sample preparation, is less accurate than the direct Ca^{2+}-ATPase measurements. Another factor limiting the accuracy of the simulation method is its sensitivity to the difference between k_1 and k_2. For the determination of k_2 to be more accurate, k_2 must be the rate-limiting step of the overall reaction. As seen with the results obtained for the posthydrolysis states, only limiting values for k_2 could be determined when the first step is slower than the second one. Nonetheless, the simulations do provide for the first time important information about the conformation and cross-linking of the SH1-SH2 helix in the transition states of S1.

When bound to S1, the transition state analog ADP.BeF_x mimics the prehydrolysis state of ATP, whereas ADP.AlF_4- and ADP.V_i are representative of the posthydrolysis state of ATP (Fisher et al., 1995). Spectroscopic and electron paramagnetic resonance studies of probes placed on SH1 have indicated that the SH1-SH2 region adopts different conformations for the pre- and posthydrolysis states of S1.ATP (Phan et al., 1997; Ponomarev et al., 1995). Consistent with this, the k_{2N}/k_2 ratios for S1.ADP.BeF_x and S1.ATPγS, another ATP-like analog, are very similar. As expected, these results suggest that ADP.BeF_x induces a similar destabilization or state of the SH1-SH2 helix as ATPγS. This also provides further support for the validity of the numerical computer method for the kinetic description of SH1-SH2 cross-linking in the S1.ADP.AlF_4- and S1.ADP.V_i states.

For the posthydrolysis states of S1.ATP, the results indicated that the SH1-SH2 may be destabilized to the point that the distance between SH1 and SH2 covers a larger length span than observed for the other states. This is surprising because the posthydrolysis state is believed to be structurally stable, primed for the swinging of the lever arm. Indeed, a stable structure of the SH1-SH2 helix was observed for S1 with the bound ADP. AlF_4- or ADP.V_i (Fisher et al., 1995; Smith and Rayment, 1996; Dominguez et al., 1998; Houdusse et al., 2000). On the other hand, Cheung et al. (1991) found a considerable decrease (~10 Å) in the mean distance between SH1 and SH2 FRET probes in the S1.ADP.V_i complex relative to S1 or acto-S1 and overall helix flexibility in all S1 states. Our cross-linking results also show considerable flexibility of this helix in the transition (analog) states of S1. With pPDM and BM, the k_{2N}/k_2 ratios for the S1.ADP.AlF_4- and S1.ADP.V_i states are at least 20-fold greater than for the nucleotide free state of S1. Because similar results were also obtained with the shorter reagent, the destabilization of the helix may be similar or greater in the posthydrolysis than in the prehydrolysis state of S1.

In contrast to the solution results, the crystal structures of S1 in the posthydrolysis states do not indicate any destabilization of the SH1-SH2 helix. This merits some consider-

ation. The experiments in this study show a range of the SH1-SH2 helix conformations (i.e., SH1-SH2 distances) for S1.ADP.AlF_4− or S1.ADP.V_i, as deduced from reactions with different size reagents (with mean cross-linking spans between ~9.4 and 14.5 Å; Table 1). Despite revealing helix destabilization in the posthydrolysis S1 state, our kinetic results do not determine the relative populations of S1 with different conformational states of the helix. A broad distribution of such states was indicated by previous FRET measurements (Cheung et al., 1991). Which of these states is crystallized may depend on their fractional population and, if any, their selection by the crystallization process. Importantly, our recent studies reveal a greater destabilization of the SH1-SH2 helix in scallop than in skeletal S1 (unpublished results). While this is consistent with the crystallization of scallop S1.ADP with the melted SH1-SH2 helix (Houdusse et al., 1999), it also shows that isoform-specific differences contribute to helix dynamics. The isoforms may affect the distribution of conformations in each nucleotide state and, through this, most likely influence which helix state is ultimately crystallized. If this is the case, accurate comparisons cannot be made between the solution properties of the skeletal S1 helix and the crystallographic structures of *Dictyostelium discoideum* and smooth muscle myosin isoforms. Nevertheless, the differences between solution results and crystal structures may be simply those between the property of a population of S1 states (in solution) and a single state stabilized in a crystal.

Although we determined the lower limits for the cross-linking rate constants for the posthydrolysis states of S1, the actual cross-linking rates in the transition state complexes of S1 could not be determined in this work. To determine the actual rates of SH1-SH2 cross-linking in the ADP.AlF_4− and ADP.V_i states of S1, other approaches should be considered. Recently, a heterobifunctional reagent, *N*-(4-azido-2-nitrophenyl) putrescine, was used to cross-link Gln-41 to Cys-374 on the adjacent monomer of the actin filament (Hegyi et al., 1998). Unlike other reactions using azido-based reagents, photocross-linking with *N*-(4-azido-2-nitrophenyl) putrescine has been shown to be ~95% efficient. Similar reagents could be synthesized for use in cross-linking experiments with S1. With such reagents, the initial attachment reaction (SH1 modification) can be separated from the subsequent cross-linking reaction. This should allow for the formation of the transition state analog complexes and the subsequent measurement of the rate of photo-activated SH2 cross-linking.

The important finding of our study is that the rates of SH1-SH2 cross-linking in the transition state S1.analog complexes are not much slower (Table 3) and may actually be equal or faster than in the S1.ADP and S1.ATPγS complexes. Thus, unlike actin binding to S1 (Nitao and Reisler, 2000), the formation of the ATP hydrolysis transition state does not stabilize the SH1-SH2 helix, at least as judged by its cross-linking. Assuming that the movement of the lever arm region of S1 can be viewed as that of a rigid body, the flexibility of the SH1-SH2 helix in the transition state could lead to the multiple orientations of the lever arm, as observed in cryo-electron microscopy and electron paramagnetic resonance studies (Walker et al., 1994, 1999; Roopnarine et al., 1998). Moreover, if myosin cross-bridges enter the power stroke step with variable orientations of the lever arm, the step sizes executed by these myosins may vary as well.

This work was supported by the National Institutes of Health Grants GM31299 (to T.O.Y.), USPHS AR22031, and NSF MCB-9904599 (to E.R.).

REFERENCES

Bradford, M. M. 1976. A rapid and sensitive method for the quantitation of microgram quantities of protein utilizing the principle of protein-dye binding. *Anal. Biochem.* 72:248–254.

Cheung, H. C., I. Gryczynski, H. Malak, W. Wiczk, M. L. Johnson, and J. R. Lakowicz. 1991. Conformational flexibility of the Cys 697-Cys 707 segment of myosin subfragment-1: distance distributions by frequency-domain fluorometry. *Biophys. Chem.* 40:1–17.

Dominguez, R., Y. Freyzon, K. M. Trybus, and C. Cohen. 1998. Crystal structure of a vertebrate smooth muscle myosin motor domain and its complex with the essential light chain: visualization of the pre-power stroke state. *Cell.* 94:559–571.

Ellman, G. L. 1959. Tissue sulfhydryl groups. *Arch. Biochem. Biophys.* 82:70–77.

Fisher, A. J., C. A. Smith, J. B. Thoden, R. Smith, K. Sutoh, H. M. Holden, and I. Rayment. 1995. X-ray structures of the myosin motor domain of *Dictyostelium discoideum* complexed with MgADP.BeFx and MgADP.AlF4. *Biochemistry.* 34:8960–8972.

Godfrey, J. E., and W. F. Harrington. 1970. Self-association in the myosin system at high ionic strength: I. Sensitivity of the interaction to pH and ionic environment. *Biochemistry.* 9:886–893.

Goodno, C. C. 1982. Myosin active-site trapping with vanadate ion. *Methods Enzymol.* 85:116–123.

Green, N. S., E. Reisler, and K. N. Houk. 2001. Quantitative evaluation of the lengths of homobifunctional protein cross-linking reagents used as molecular rulers. *Protein Sci.* 10:1293–1304.

Gulick, A. M., C. B. Bauer, J. B. Thoden, and I. Rayment. 1997. X-ray structures of the MgADP, MgATPγS, and MgAMPPNP complexes of the *Dictyostelium discoideum* myosin motor domain. *Biochemistry.* 36: 11619–11628.

Hegyi, G., M. Mák, E. Kim, M. Elzinga, A. Muhlrad, and E. Reisler. 1998. Intrastrand cross-linked actin between Gln-41 and Cys-374: I. Mapping of sites cross-linked in F-actin by *N*-(4-azido-2-nitrophenyl) putrescine. *Biochemistry.* 37:17784–17792.

Hiratsuka, Y., M. Eto, M. Yazawa, and F. Morita. 1998. Reactivities of Cys707 (SH1) in intermediate states of myosin subfragment-1 ATPase. *J. Biochem.* 124:609–614.

Houdusse, A., V. N. Kalabokis, D. Himmel, A. G. Szent-Györgyi, and C. Cohen. 1999. Atomic structure of scallop myosin subfragment S1 complexed with MgADP: a new conformation for the myosin head. *Cell.* 97:459–470.

Houdusse, A., A. G. Szent-Györgyi, and C. Cohen. 2000. Three conformational states of scallop myosin S1. *Proc. Natl. Acad. Sci. U. S. A.* 97:11238–11243.

Kinose, F., S. X. Wang, U. S. Kidambi, C. L. Moncman, and D. A. Winkelmann. 1996. Glycine 699 is pivotal for the motor activity of skeletal muscle myosin. *J. Cell. Biol.* 134:895–909.

Marriott, G., and M. Heidecker. 1996. Light-directed generation of the actin-activated ATPase activity of caged heavy meromyosin. *Biochemistry*. 35:3170–3174.

Nitao, L. K., and E. Reisler. 1998. Probing the conformational states of the SH1-SH2 helix in myosin: a cross-linking approach. *Biochemistry*. 37: 16704–16710.

Nitao, L. K., and E. Reisler. 2000. Actin and temperature effects on the cross-linking of the SH1-SH2 helix in myosin subfragment 1. *Biophys. J.* 78:3072–3080.

Patterson, B., K. M. Ruppel, Y. Wu, and J. A. Spudich. 1997. Cold-sensitive mutants G680V and G691C of *Dictyostelium* myosin II confer dramatically different biochemical defects. *J. Biol. Chem*. 272: 27612–27617.

Phan, B. C., P. Cheung, W. F. Stafford, and E. Reisler. 1996. Complexes of myosin subfragment-1 with adenosine diphosphate and phosphate analogs: probes of active site and protein conformation. *Biophys. Chem.* 59:341–349.

Phan, B. C., Y. M. Peyser, E. Reisler, and A. Muhlrad. 1997. Effect of complexes of ADP and phosphate analogs on the conformation of the Cys707-Cys697 region of myosin subfragment 1. *Eur. J. Biochem.* 243:636–642.

Polosukhina, K., and S. Highsmith. 1997. Kinetic investigation of the ligand dependence of rabbit skeletal muscle myosin subfragment 1 Cys-697 and Cys-707 reactivities. *Biochemistry*. 36:11952–11958.

Ponomarev, M. A., V. P. Timofeev, and D. I. Levitsky. 1995. The difference between ADP-beryllium fluoride and ADP-aluminium fluoride complexes of the spin-labeled myosin subfragment 1. *FEBS Lett.* 371: 261–263.

Reisler, E., M. Burke, S. Himmelfarb, and W. F. Harrington. 1974. Spatial proximity of the two essential sulfhydryl groups of myosin. *Biochemistry*. 13:3837–3840.

Riddles, P. W., R. L. Blakeley, and B. Zerner. 1983. Reassessment of Ellman's reagent. *Methods Enzymol*. 91:49–60.

Roopnarine, O., A. G. Szent-Györgyi, and D. D. Thomas. 1998. Microsecond rotational dynamics of spin-labeled myosin regulatory light chain induced by relaxation and contraction of scallop muscle. *Biochemistry*. 37:14428–14436.

Root, D. D., and E. Reisler. 1992. Cooperativity of thiol-modified myosin filaments: ATPase and motility assays of myosin function. *Biophys. J.* 63:730–740.

Sekine, T., and W. W. Kielley. 1964. The enzymatic properties of *N*-ethylmaleimide modified myosin. *Biochim. Biophys. Acta*. 81:336–345.

Smith, C. A., and I. Rayment. 1996. X-ray structure of the magnesium-(II).ADP.vanadate complex of the *Dictyostelium discoideum* myosin motor domain to 1.9 A resolution. *Biochemistry*. 35:5404–5417.

Spudich, J. A., and S. Watt. 1971. The regulation of rabbit skeletal muscle contraction: I. Biochemical studies of the interaction of the tropomyosin-troponin complex with actin and the proteolytic fragments of myosin. *J. Biol. Chem.* 246:4866–4871.

Walker, M., H. White, B. Belknap, and J. Trinick. 1994. Electron cryomicroscopy of acto-myosin-S1 during steady-state ATP hydrolysis. *Biophys. J.* 66:1563–1572.

Walker, M., X. Z. Zhang, W. Jiang, J. Trinick, and H. D. White. 1999. Observation of transient disorder during myosin subfragment-1 binding to actin by stopped-flow fluorescence and millisecond time resolution electron cryomicroscopy: evidence that the start of the crossbridge power stroke in muscle has variable geometry. *Proc. Natl. Acad. Sci. U. S. A.* 96:465–470.

Weeds, A. G., and B. Pope. 1977. Studies on the chymotryptic digestion of myosin: effects of divalent cations on proteolytic susceptibility. *J. Mol. Biol.* 111:129–157.

Wells, J. A., C. Knoeber, M. C. Sheldon, M. M. Werber, and R. G. Yount. 1980. Cross-linking of myosin subfragment 1: nucleotide-enhanced modification by a variety of bifunctional reagents. *J. Biol. Chem.* 255: 11135–11140.